Order-by-disorder from Schwinger bosons in a frustrated honeycomb ferromagnet

Arnaud Ralko¹ and Jaime Merino²

¹Institut Néel, Université Grenoble Alpes and CNRS, Grenoble, France ²Departamento de Física Teórica de la Materia Condensada, Condensed Matter Physics Center (IFIMAC) and Instituto Nicolás Cabrera, Universidad Autónoma de Madrid, Madrid 28049, Spain (Dated: 21 novembre 2025)

The cobalt-based honeycomb magnet $\mathrm{BaCo_2(AsO_4)_2}$ (BCAO) has recently emerged as a promising platform for studying frustrated magnetism beyond conventional paradigms. Neutron-scattering experiments and first-principles calculations have revealed an unexpected double-zigzag (dZZ) magnetically ordered ground state, whose microscopic origin remains under active debate. Here, we investigate the emergence of such dZZ phase in a ferro–antiferromagnetic J_1-J_3 Heisenberg model on the honeycomb lattice using a generalized Schwinger-boson mean-field theory (g-SBMFT) that treats ferromagnetic and antiferromagnetic interactions on equal footing. Based on g-SBMFT and exact-diagonalization (ED) techniques, we find that the dZZ is selected by an order-by-disorder mechanism in a narrow $J_3/|J_1|$ range, in agreement with recent density-matrix renormalization-group calculations. The magnetic excitation spectra within the dZZ phase displays a distinctive smearing out in momentum space due to quantum fluctuations which may be probed through inelastic neutron-scattering experiments.

I. INTRODUCTION

The investigation of frustrated magnetism on honeycomb materials has been fueled in the last decade or so by the search of the Kitaev spin liquid (KSL). The KSL is characterized by exotic excitations such as \mathbb{Z}_2 gauge fluxes and itinerant Majorana fermions, as well as an anomalous thermal Hall effect under an external magnetic field. Although the Ru-based material, α -RuCl₃, was first thought as an ideal platform for Kitaev physics, other interactions drive the material to more conventional magnetically ordered phases [1–4]. This has motivated the search for alternative Kitaev materials such as the cobaltates [5] which, in spite of hosting a weaker spinorbit coupling (SOC) than their Ru(5d) and Ir(4d) counterparts, they realize the Kitaev bond-dependent interactions [6, 7]. In this regard, BaCo₂(AsO₄)₂ (BCAO) is possibly the most promising Co-based honeycomb magnet to host a KSL. Elastic magnetic scattering on this 3d⁷ candidate KSL material indicates that is an incommensurate antiferromagnet (AFM) [8] for $T < T_N = 5.35$ K with ordering wavevector $\mathbf{q}_1 = (0.27, 0, -1.31)$. At $T < T_N$ under an external magnetic field $\mu_0 H \approx \mu_0 H_{c1} = 0.33$ T along the honeycomb in-plane b-direction, BCAO undergoes a transition to commensurate magnetic order $\mathbf{q}_2 = (1/3, 0, -1.31)$ which becomes almost fully polarized at $\mu_0 H_{c2} = 0.55$ T. On the other hand, inelastic neutron scattering (INS) experiments on BCAO at T = 1.5K find a characteristic gapped flat mode [7] with a minimum at the Γ -point instead of displaying the expected Goldstone mode at \mathbf{q}_1 . This observation together with the extremely small T_N and H_{c2} suggest that BCAO is lying close to a ferromagnetic (FM) transition in 2D

In spite of the amount of work devoted to BCAO and cobaltates in general, constructing a minimal model with captures all their fascinating magnetic proper-

ties has remained elusive. Previous works combining ab initio calculations [9] with experimental observations [10– 13] support an XXZ- J_1 - J_3 , with FM $J_1 < 0$ and AFM $J_3 > 0$, and additional third neighbor off-diagonal couplings, $J_{z+}^{(3)}$, (expressed in the crystallographic frame) as a minimal model for BCAO. The ground state of this model is an unconventional uudd or double zig-zag (dZZ) state when $J_3/|J_1| \sim 0.2 - 0.4$ and the off-diagonal $J_{z\pm}^{(3)} \neq 0$. However, very recent refinements have raised the importance of Kitaev bond-dependent exchange interactions [6] in order to capture the full details observed in INS experiments on BCAO. Monte-Carlo simulations on a J_1 - $K-\Gamma-\Gamma'-J_2-J_3$ model reconcile the nearly perfect dZZ order with the incommensurate magnetism observed and the gap, $\Delta \sim 1.45$ meV, at the ab-plane Γ -point in INS spectra. These calculations show how the absence of the Goldstone mode [7] can be ascribed to defective dZZ order. The common thread of these minimal models is that they can accommodate dZZ order or their closely related versions. Since the dZZ is a compromise between FM and a zig-zag (ZZ) state, it is extremely sensitive to tiny magnetic fields going through a transition to an intermediate *uud* state before becoming fully polarized. This can explain the 1/3 magnetization plateau experimentally observed for : $H_{c1} < H < H_{c2}$.

Motivated by recent DMRG calculations of the ferroantiferromagnetic J_1 - J_3 Heisenberg model on the honeycomb lattice revealing an order-by-disorder mechanism [14] underlying the stabilization of the dZZ, we explore the possibility that such "simple" model contains the essential ingredients to describe magnetic properties of BCAO. Using g-SBMFT and ED techniques, we show how a dZZ state indeed can emerge in this model. Since the standard SBMFT [15] (s-SBMFT from now on) has been mostly applied to frustrated antiferromagnetic models [16, 17], we introduce an extension which can handle frustrated ferromagnetic models, avoiding previous difficulties [18] associated with the violation of the boson number constraint. The phase dia-

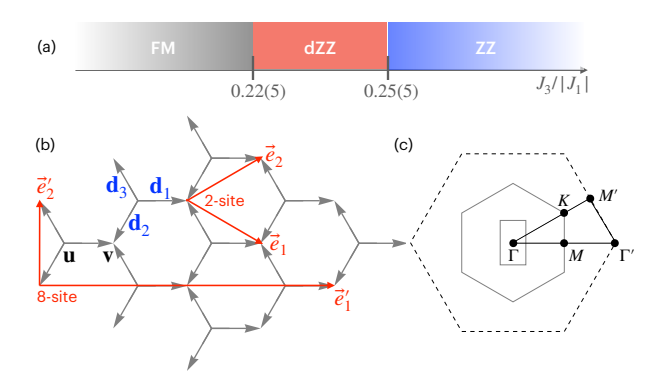


FIGURE 1. (a) Phase diagram of the ferro-antiferromagnetic J_1 - J_3 model at T=0. (b) Honeycomb lattice with two sublattices u and v, and the three nearest-neighbor displacement vectors $\{\mathbf{d_i}\}$ for a 2-site unit-cell and its primitive vectors $(\mathbf{e_1}, \mathbf{e_2})$, and for an 8-site unit-cell with $(\mathbf{e_1'}, \mathbf{e_2'})$. (c) Corresponding first (solid lines) and second (dashed lines) Brillouin zones together with high-symmetry points. The dynamical structure factors are analyzed along the path $K\Gamma M\Gamma' M' K\Gamma$.

gram of the model obtained from this g-SBMFT shown in Fig. 1(a), displays a FM and a ZZ phase as expected classically. Interestingly, a dZZ state occurs at intermediate $J_3/|J_1| \sim 0.22(5) - 0.25(5)$ in very good agreement with previous DMRG results on finite cylinders [14]. Our work supports the idea that the dZZ phase in the J_1 - J_3 model is indeed stabilized by quantum fluctuations through an order-by-disorder mechanism, as proposed recently [14]. It also reveals the non-trivial structure of this peculiar magnetic order through the Schwinger boson language. In order to make contact with experiments, we calculate the magnetic excitation spectra of the different phases. While minima in the magnon dispersion occur at the Mand M/2-points in the ZZ and dZZ phases as expected, a strong spectral weight redistribution between the 1st and 2nd Brillouin Zones (BZ) occurs in the gapped QSL phases which may be relevant to experiments.

The remainder of this paper is organized as follows. In Sec. II we introduce the ferro-antiferromagnetic J_1 J_3 Heisenberg model on the honeycomb lattice and describe in detail the generalized Schwinger-boson meanfield theory (g-SBMFT) developed to treat competing ferromagnetic and antiferromagnetic couplings on an equal footing. In Sec. III we present the resulting meanfield spinon structures and discuss the characteristic Ansätze corresponding to the ZZ and dZZ magnetic orders, emphasizing the role of triplet pairing terms in stabilizing the latter. Section IV establishes the groundstate phase diagram by comparing the g-SBMFT results with conventional s-SBMFT and exact-diagonalization calculations. This section also highlights the emergence of the dZZ phase through a quantum order-by-disorder mechanism[14] and analyzes the associated real-space spin-correlation patterns. In Sec. V we compute the

dynamical magnetic excitation spectra within both ZZ and dZZ phases, identifying distinctive redistributions of spectral weight across Brillouin zones and discussing their relevance to recent inelastic neutron-scattering observations on $BaCo_2(AsO_4)_2$. Finally, Sec. VI summarizes our main conclusions and outlines possible extensions of the present work, including the effects of external magnetic fields, bond-dependent exchange terms, and structural disorder on the stability of the dZZ phase.

II. MODEL AND METHODS

We consider the honeycomb lattice where, as shown in Fig. 1(b), each lattice site of the u sublattice is connected to three v sublattice nearest neighbors through the bond vectors $\mathbf{d}_{1,2,3}$. As it will become clearer in the next section, we consider two types of unit-cells, with 2 and 8 sites (Fig. 1(c)), whose respective first Brillouin zones are displayed in panel (c).

We investigate an isotropic Heisenberg model with interactions extending beyond nearest neighbors. Quantum spins \mathbf{S}_i occupy each lattice site i, and the Hamiltonian is given by

$$\mathcal{H} = \sum_{\langle i,j \rangle} \hat{\mathbf{S}}_i J_1 \hat{\mathbf{S}}_j + \sum_{\langle \langle \langle i,j \rangle \rangle \rangle} \hat{\mathbf{S}}_i J_3 \hat{\mathbf{S}}_j, \tag{1}$$

where the first sum runs over nearest-neighbor pairs and the second over third-neighbor pairs. Both J_1 and J_3 preserve full spin-rotation symmetry, in contrast to bond-dependent couplings that reduce lattice [6, 9, 10]. The competition between the ferromagnetic, $J_1 < 0$, and the AFM, $J_3 > 0$, can lead to frustration in a $J_3/|J_1|$ parameter range which we explore here.

We analyze Eq. (1) within the Schwinger-boson meanfield theory (SBMFT) framework [15, 16], a method that has been extensively applied to frustrated antiferromagnetic (AF) Heisenberg models [17, 19–23]. Prominent examples include the AF J_1 - J_2 model on the square lattice [24] as well as the triangular, kagome [17, 25], and honeycomb lattices [26, 27]. In contrast, systems involving both ferromagnetic (FM) and antiferromagnetic (AFM) couplings have been much less explored within the SBMFT framework, mainly because obtaining stable mean-field solutions in the FM regime is notoriously difficult without invoking Bose condensation of the Schwinger bosons. Our present model, Eq. (1), explicitly includes competing FM and AFM interactions on the honeycomb lattice, thereby extending the applicability of SBMFT to a regime rarely addressed in previous studies, apart from e.g. related work on the square lattice [18, 28] or ferrimagnetism on 1D-chain [29], or by considering further advanced theoretical developments [30–33].

In the Schwinger boson representation, the spin operator at site i is expressed as

$$\hat{\mathbf{S}}_i = \frac{1}{2} \hat{b}_i^{\dagger} \boldsymbol{\sigma} \hat{b}_i, \tag{2}$$

where $\hat{b}_i^{\dagger} = (\hat{b}_{i,\uparrow}^{\dagger}, \hat{b}_{i,\downarrow}^{\dagger})$, the boson spinor, creates bosonic spinons, and $\boldsymbol{\sigma} = \sigma^1 \mathbf{u}_x + \sigma^2 \mathbf{u}_y + \sigma^3 \mathbf{u}_z$ denotes the Pauli matrices. We also define σ^0 as the 2×2 identity matrix, with $\alpha = 0, 1, 2, 3$ labeling the components.

To reproduce the correct spin- $\!S$ algebra, one must impose the boson-number constraint

$$\hat{n}_i = \hat{b}_i^{\dagger} \hat{b}_i = 2S = \kappa, \tag{3}$$

which projects out unphysical states. While exact enforcement would render the representation faithful, in practice it is too complicated [34] and the constraint is implemented on average via site-dependent Lagrange multipliers:

$$\sum_{i} \lambda_{i} \left(\hat{n}_{i} - \kappa \right), \tag{4}$$

added to the Hamiltonian. This treatment allows one to view S (or κ) as a parameter controlling the strength of quantum fluctuations, an advantage allowing us to explore the quantum melting of magnetic ordered states and see to which quantum spin liquid states they are related.

The Hamiltonian (1) contains only SU(2)-invariant Heisenberg terms that take the generic form,

$$\hat{\mathbf{S}}_{i}\hat{J}\hat{\mathbf{S}}_{j} = \frac{1}{4}J_{\alpha,\beta}T_{s_{0}s_{1}s_{2}s_{3}}^{\alpha\beta}\hat{b}_{i,s_{0}}^{\dagger}\hat{b}_{i,s_{1}}\hat{b}_{j,s_{2}}^{\dagger}\hat{b}_{j,s_{3}}, \quad (5)$$

where repeated indices are summed up, J is the 3×3 coupling matrix on the bond (i,j), and $T^{\alpha\beta}_{s_0s_1s_2s_3}=\sigma^{\alpha}_{s_0,s_1}\sigma^{\beta}_{s_2,s_3}$ is a rank-4 tensor. Up to this stage, the parton construction remains exact, independent of the form of J.

To proceed further, we decouple quartic operators into mean-field channels of pairing and hopping bond operators of type :

$$\begin{split} \hat{b}_{i,s_0}^{\dagger} \hat{b}_{i,s_1} \hat{b}_{j,s_2}^{\dagger} \hat{b}_{j,s_3} \; &\rightarrow \; (b_{i,s_0}^{\dagger} b_{j,s_2}^{\dagger} \, | \, b_{i,s_1} b_{j,s_3}) \\ &= \; (\hat{p}_{ij}^{s_0 s_2 +} \, | \, \hat{p}_{ij}^{s_1 s_3}) \\ &\rightarrow \; (b_{i,s_1} b_{j,s_2}^{\dagger} \, | \, b_{i,s_0}^{\dagger} b_{j,s_3}) \\ &= \; (\hat{h}_{ij}^{s_1 s_2 +} \, | \, \hat{h}_{ij}^{s_0 s_3}), \end{split}$$

where $(\hat{A}|\hat{B}) = \langle \hat{A}\rangle\hat{B} + \hat{A}\langle\hat{B}\rangle - \langle \hat{A}\rangle\langle\hat{B}\rangle$ and where we have introduced corresponding pairing $p_{ij} = \langle \hat{p}_{ij}\rangle$ and hopping $h_{ij} = \langle \hat{h}_{ij}\rangle$ as mean-field variational parameters. Additional symmetry constraints can be enforced on the mean-field vectors, reducing the generalized decoupling to various SBMFT forms. For example, the s-SBMFT with singlet pairing and spinon hopping terms can be realized by imposing the structure:

$$\mathbf{p}_{ij} = (0, r, -r, 0), \quad \mathbf{h}_{ij} = (s, 0, 0, s).$$

where r and s are complex numbers to be determined self-consistently. Defined this way, this SBMFT formulation is more general than the usual one since it does not

anticipate any specific forms for the operators, and all possible spin combinations can be active in the theory. In particular, one could deal with singlet or triplet pairing/hopping independently, and consider any kind of spin couplings on a given bond. This includes recent works where more than two operators (singlet pairing and spinon hopping) were considered, necessary when dealing with e.g. Dzyaloshinskii-Moriya [35–38] of anisotropic interactions like in Kitaev systems [21, 39, 40].

More details on the theory are provided in the appendices.

Solving the resulting mean-field hamiltonian self-consistently, a saddle point is reached at which the corresponding Ansatz should satisfy the relation : $\langle (\hat{A}|\hat{B})\rangle = \langle \hat{A}\rangle\langle \hat{B}\rangle$. Hence, a valid Ansatz, should simultaneously satisfy this relation as well as the boson constraint Eq. (3).

A key aspect of the present model is that it contains both ferromagnetic J_1 and antiferromagnetic J_3 interactions. In the s-SBMFT treatment of the T = 0 FM Heisenberg model all bosons are condensed at the Γ point consistent with the expected classical FM order. Self-consistent approaches trying to reproduce such state on finite lattices fail since only FM-type hopping amplitudes, i. e. the triplet h_{ij} amplitudes, are non-zero leading to a SBMFT vacuum that violates the boson number constraint. In the generalized SBMFT (q-SBMFT) introduced here, triplet pairing amplitudes describing FM may not vanish allowing for a description of FM on finite lattices with the required number of bosons per site. Hence, the g-SBMFT has the potential of describing more complex magnetic states since it involves combinations of singlet and triplet operators in both pairing and hopping channels [39]. We follow this route here and compare sand g-SBMFT results whenever possible.

III. MEAN-FIELD SPINON STRUCTURES

Here we introduce the relevant spinon Ansätze used in the present study of model (1) and analyze their meanfield structure as well as spinon dispersion relations.

Figure 2 displays the mean-field spinon sign patterns corresponding to the ZZ and dZZ Ansätze, as obtained within both the s-SBMFT [panel (a)] and g-SBMFT [panels (b,c)] frameworks. In the conventional s-SBMFT formulation, all bonds—FM and antiferromagnetic alike—are described in terms of singlet pairing p_0 and spinon hopping h_0 . In contrast, the g-SBMFT Ansatz exhibits a crucial distinction: for ferromagnetic bonds, it is the triplet pairing amplitudes $p_{2,3}$ that acquire finite expectation values. This allows finding stable selfconsistent ZZ and dZZ solutions with converged energies satisfying the boson number constraint. We find the sequence of phase transitions with increasing J_3 going from a ferromagnetic state at low J_3 to the dZZ phase and finally to the ZZ phase in agreement with previous analysis [6, 9, 10, 14]. Since the intermediate dZZ phase does not match any of the energetically favourable classical

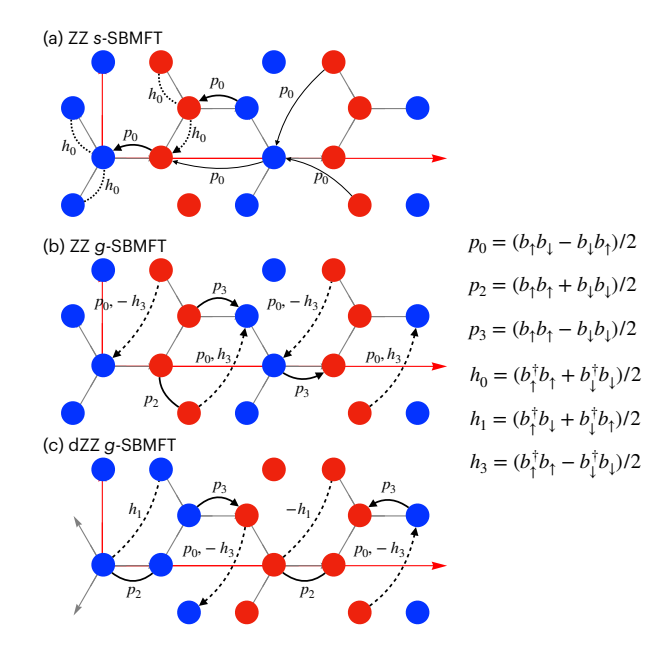


FIGURE 2. Ansätze of the ZZ and the dZZ structures within the s- and g-SBMFT frameworks. (a) Mean-field structure of the ZZ phase obtained from the s-SBMFT. Despite ferromagnetic nearest-neighbor bonds, nonzero singlet pairings are present. (b) Corresponding ZZ Ansatz obtained from the g-SBMFT, where ferromagnetic bonds (solid lines) host nonzero triplet pairings $P_{2,3} \neq 0$, while antiferromagnetic J_3 bonds (dashed lines/arrows) carry both singlet p_0 and triplet hopping amplitudes h_3 . This Ansatz achieves a lower energy than (a); see text for discussion. (c) Structure of the dZZ phase, accessible only within the g-SBMFT formalism and on the 8-site unit-cell.

orders, it is then selected by the quantum fluctuations. Hence, the g-SBMFT predicts a small but finite J_3 range where the mechanism of quantum order-by-disorder becomes operative corroborating previous DMRG findings on smaller systems [14].

In Fig. 3 we show the lowest energy spinon dispersions of the ZZ phase obtained within s-SBMFT on a twosite [panel (a)] and eight-site [panel (b)] unit cells for S = 0.35 and $J_3 = 1$. The These can be compared with the g-SBMFT lowest energy spinon dispersions of the ZZ [panel (c)] and dZZ [panel (d)] phases. All energy spinon dispersions exhibit the characteristic stripe-like modulation associated with the periodic arrangement of magnetically ordered vertical stripes of the ZZ and dZZ phases. The s-SBMFT lowest energy spinon dispersion for the ZZ phase in the 2-site unit cell shown in (a) displays a minimum at $\mathbf{Q}/2 = \pm (\pi/\sqrt{3}a, 0)$ inside the 1BZ, where \mathbf{Q} denotes the ZZ ordering wavevector. On the other hand, in the eight-site cell, which can accommodate both the ZZ and dZZ periodicities, the lowest energy spinon dispersion minimum is located at the Γ point of the reduced BZ (see Fig. 1).

The lowest energy spinon dispersions of the ZZ phase obtained from the s-SBMFT and g-SBMFT Ansätze are

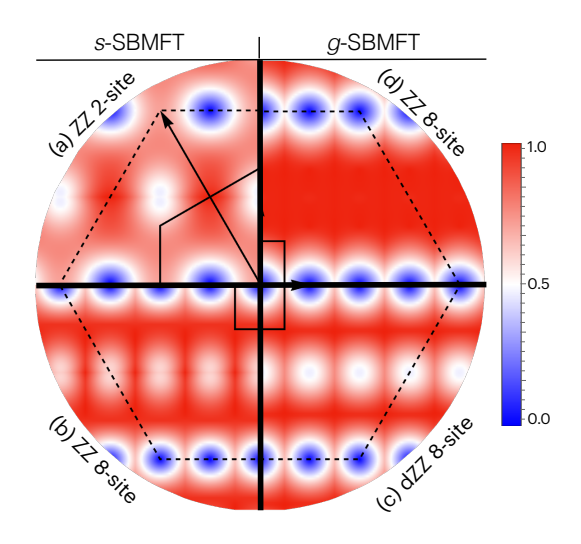


FIGURE 3. Lowest-energy spinon dispersions for (a) the ZZ phase obtained from s-SBMFT on a two-site unit cell with S=0.35 and $J_3=1.0$, (b) the same ZZ Ansatz on an eight-site unit cell, and (c,d) the ZZ and dZZ Ansätze from g-SBMFT on the same eight-site cell. For all cases, only one quarter of the first (solid lines) and second (dashed lines) Brillouin zones shown in Fig. 1 are shown.

compared in panels (b) and (c). Although the overall structure is similar small differences can also be noticed. On the other hand, the g-SBMFT lowest energy spinon dispersions of the ZZ [panel (c)] and dZZ [panel (d)] on the 8-site unit cell show different structures particularly in the momentum region between the zero spinon modes. This is consistent with the quite different sign patterns of the mean-field parameters encoded in the two Ansätze (compare Fig. 7(b) and (c)).

IV. PHASE DIAGRAM

We have obtained the phase diagram of model (1) based on the s- and g-SBMFT on an 8-site unit cell compatible with all possible Ansätze presented in the previous section, up to linear cluster sizes l=12. We also provide ED calculations on 24-site hexagonal clusters (see Appendix E) with PBC for comparison.

A significant difference between the two mean-field approaches emerges when considering the dZZ phase. Within the s-SBMFT, we have been unable to find a self-consistent dZZ solution. This may be attributed to the fact that each spin is ferromagnetically coupled to all three nearest neighbors in the dZZ phase similar to the FM case. In contrast, the g-SBMFT formulation introduced here allows for linear combinations of singlet and triplet components in both pairing and hopping channels, thereby significantly enlarging the variational space. This extension enables a self-consistent energetically stable dZZ solution occurring in a narrow parameter range between the FM and ZZ phases. These findings

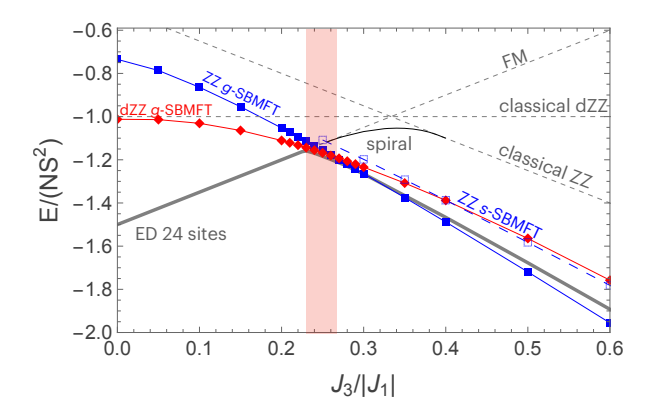


FIGURE 4. Dependence of the ground state energy of the ferroantiferromagnetic J_1 - J_3 Heisenberg model on J_3 . Energies obtained from ED (thick solid gray line) for the model with S=1/2 are compared with our g-SBMFT approach with S=0.25 (symbols). Results are shown for the ZZ (red) and dZZ (blue) Ansätze, and compared with the ZZ solution obtained from the conventional s-SBMFT (dashed blue line). Dashed gray lines indicate the classical energies of the FM, dZZ and ZZ orders. The red shaded region marks the finite parameter window in which the dZZ phase is selected through order-by-disorder. Energies per site normalized to S^2 for fixed $J_1=-1$ are shown in this plot.

are consistent with recent DMRG studies performed on long cylinders [14] and our ED calculations as discussed below

In Fig. 4 we show the ground-state energy dependence on J_3 obtained from s- and g-SBMFT, ED and classically. Since the spin length S effectively controls the magnitude of quantum fluctuations in the SBMFT approaches, the energy per site is rescaled by S^2 for a meaningful comparison across methods. As discussed above, the s-SBMFT treatment on finite systems fails to reproduce the FM state without violating the boson-number constraint, as this state is classical. Similarly, the g-SBMFT approach can neither capture the FM phase despite its broader parameter space. Hence, we assume the exact classical energy dependence on J_3 in the FM phase. Through the comparison with the energies in the ZZ and dZZ phases we can determine the various phase transitions in the model. The much lower ED energy compared to the classical energy found for $J_3/|J_1| \gtrsim 0.225$, i.e. above the FM phase, indicates the prominent role played by quantum fluctuations. For instance, quantum fluctuations extend the parameter range in which the ZZ state stable to lower $J_3/|J_1|$. Crucially, the dZZ state instead of the spiral phase found classically emerges between FM and ZZ states.

The g-SBMFT energies shown in Fig. 4 show how the dZZ phase becomes energetically more favorable over the ZZ phase for $J_3/|J_1|\lesssim 0.255$, while the FM state attains the lowest energy for $J_3/|J_1|\lesssim 0.225$. The dependence of energy on $J_3/|J_1|$ obtained from g-SBMFT closely follows the ED energies, lending further support to the approach.

From these results we conclude that the dZZ phase is stable in the parameter range $0.225 \lesssim J_3/|J_1| \lesssim 0.255$ from g-SBMFT. This parameter range is also in good agreement with ED results of $S(\mathbf{q})$ as discussed below. Fig. 4 also reveals that the ZZ state obtained from g-SBMFT attains a lower energy than its s-SBMFT counterpart. This shows the improved variational flexibility gained by incorporating both singlet and triplet channels in the SBMFT. Moreover, the g-SBMFT energies show markedly better agreement with ED results in the range of $J_3/|J_1|$ shown. It is worth noting that, since the SBMFT framework is intrinsically non-variational, the mean-field energies can occasionally lie slightly below those obtained from ED.

From our $T=0{\rm K}$ ground state energy analysis we find that quantum fluctuations favor dZZ order which is none of the ground states predicted classically for any $J_3/|J_1|$. Hence, we conclude that an order-from-disorder mechanism mediated by quantum fluctuations is responsible for selecting the dZZ phase as a compromise between the FM and ZZ phases.

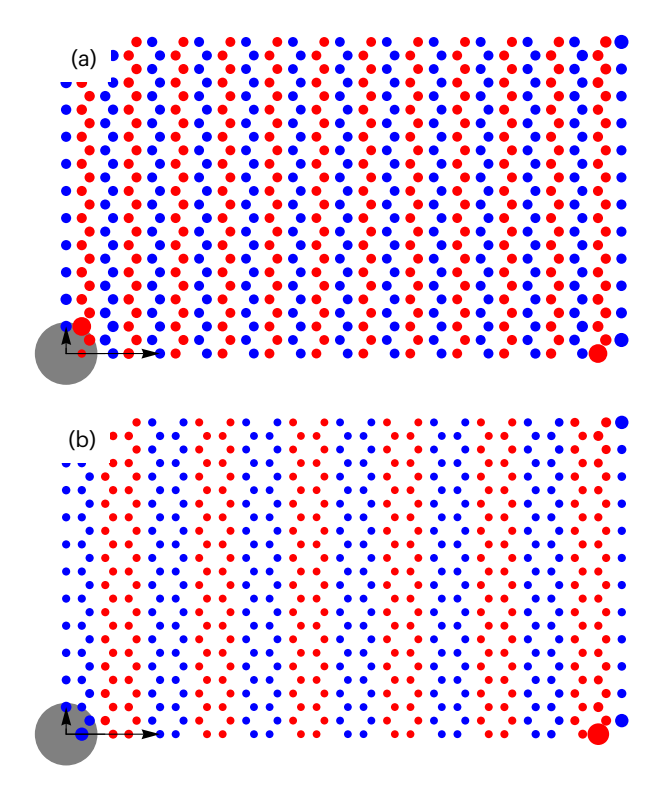


FIGURE 5. Real space spin-spin correlations for (a) the ZZ and (b) the dZZ phases, calculated for $\kappa=0.5$ at $J_3/|J_1|=0.3$ on a $8\times 6\times 6$ site cluster. The size of the disk corresponds to the strength of the correlation (in arbitrary units) and the colors correspond to positive (blue), negative (red) correlations and the reference site is at the lower-left corner (gray). Black arrows show the translation vectors of the 8-site unit-cell compatible with all ordered phases of the present work.

Further understanding of the role played by quantum fluctuations in our model (1) can be achieved through

the analysis of real space spin correlations in the ground state. We define spin correlations as :

$$C(\mathbf{r}_i - \mathbf{r}_j) = \langle \mathbf{S}_i \cdot \mathbf{S}_j \rangle, \tag{6}$$

which capture the spatial arrangement of the spins.

In Fig. 5, we show results of $C(\mathbf{r}_0 - \mathbf{r}_i)$ normalized by S(S+1), using the g-SBMFT method both in the ZZ (a) and dZZ (b) phases for $J_3/|J_1| = 0.3$. In this parameter regime, the dZZ is the ground state of the model in the g-SBMFT method as shown in Fig. 4. In these plots, the size of the circles represents the magnitude of the correlation with respect to the lower left corner site, while the color encodes its sign (blue for positive FM correlation, red for negative AFM correlation). Two key features are immediately apparent. First, the ZZ exhibits a more robust magnetic order than the dZZ phase, the latter being closer to a classical ferromagnetic arrangement where quantum fluctuations play a negligible role. Second, the double zig-zag correlations display a clear spatial modulation in both intensity and pattern, reminiscent of the classical spiral order predicted by the Luttinger-Tisza analysis[14].

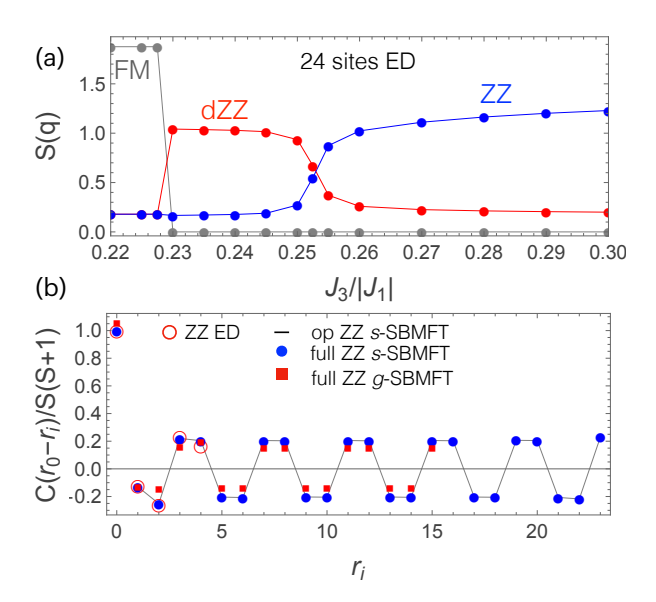


FIGURE 6. (a) Static spin structure factors obtained from ED on a 24-site (8 × 3) cluster at representative ${\bf q}$ points in the Brillouin zone : Γ (gray), M (red), and M/2 (blue), corresponding respectively to the dominant Bragg peaks of the FM, dZZ, and ZZ phases. (b) Real-space spin–spin correlations for the ZZ phase. Results are shown for S=0.5 at $J_3/|J_1|=1$, computed within the s-SBMFT using (i) the operator formulation (gray line) and (ii) the full vacuum calculation (blue dots). Also shown are results from the g-SBMFT (red squares) for S=0.25 and $J_3/|J_1|=1$, evaluated in the bosonic vacuum, and from ED on a 24-site (8 × 3) cluster (red circles) for comparison.

Figure 6(a) displays the static spin structure factors

$$S(\mathbf{q}) = \frac{1}{N} \sum_{i,j} e^{i\mathbf{q} \cdot (\mathbf{r}_i - \mathbf{r}_j)} \langle \mathbf{S}_i \cdot \mathbf{S}_j \rangle, \tag{7}$$

with N the number of sites in the system, obtained from exact diagonalization (ED) on a 24-site $(8 \times 3, \text{ see Ap-}$ pendix D for details) cluster at representative q points in the Brillouin zone : Γ (gray), M (red), and M/2(blue), corresponding respectively to the dominant Bragg peaks of the FM, dZZ, and ZZ phases. Even for such a modest cluster size, the presence of the dZZ phase is clearly evidenced, and its extent as a function of J_3 closely matches the values reported in the literature [14] as well as those obtained from our g-SBMFT analysis. Panel (b) shows the real-space spin-spin correlation function $C(\mathbf{r}_0 - \mathbf{r}_i) = \langle \mathbf{S}_0 \cdot \mathbf{S}_i \rangle$ for the ZZ phase, computed within both the conventional s-SBMFT and the present generalized g-SBMFT. The expected antiferromagnetic alignment along the armchair direction and ferromagnetic correlations along the zigzag chains confirm the characteristic ZZ ordering pattern. $C(\mathbf{r}_0 - \mathbf{r}_i)$ was evaluated using both the operator formulation and a full calculation in the bosonic vacuum (see Appendices for details). In the s-SBMFT, the two approaches yield identical results, as illustrated in the figure. However, for the new ZZ phase obtained within the g-SBMFT, the operator formulation cannot be applied directly because distinct mean-field operators act on ferromagnetic and antiferromagnetic bonds, leaving the full vacuum formulation as the appropriate and most general method. This latter formulation is expected to be the most relevant for any extended SBMFT, and a systematic comparison between the two is provided in the Appendices. Finally, comparison with ED results on the 24-site $(8 \times 3 \text{ shown in Appen-}$ dix D) cluster reveals very good quantitative agreement, particularly in the decay and oscillatory behavior of the correlations with distance. Also one can notice from Fig. fig :realspacecorrsbmft (a) how the g-SBMFT reproduce the ED spin correlations of the zz phase almost exactly near the reference site.

Altogether, the g-SBMFT framework introduced here is in agreement with ED and DMRG results. This provides further support to the order-from-disorder mechanism underlying the existence of the dZZ phase in the ferro-antiferromagnetic J_1 - J_3 Heisenberg model since our results are obtained in much larger systems. Our work also shows how the g-SBMFT is a better suited method than the s-SBMFT to deal with the magnetic properties of frustrated ferromagnets.

V. DYNAMICAL MAGNETIC EXCITATION SPECTRA

Although the SBMFT approach used here leads to a gap in the spinon spectra avoiding Boson condensation, magnetic order may still be inferred from finite-size scaling by studying the behavior of the Goldstone mode precusor, which appears at the condensation wave vector, \mathbf{Q} , with increasing size of the system. This manifests both in the static structure factor, $S(\mathbf{q})$, defined in (7) and the

dynamical structure factor:

$$S(\mathbf{q},\omega) = \frac{1}{2\pi N} \sum_{i,j} e^{i\mathbf{q}\cdot(\mathbf{r}_i - \mathbf{r}_j)} \int_{-\infty}^{\infty} dt \, e^{i\omega t} \langle \mathbf{S}_i(t) \cdot \mathbf{S}_j(0) \rangle.$$
(8)

In the presence of incipient magnetic order, $S(\mathbf{q})$ develops precursor Bragg peaks at \mathbf{Q} .

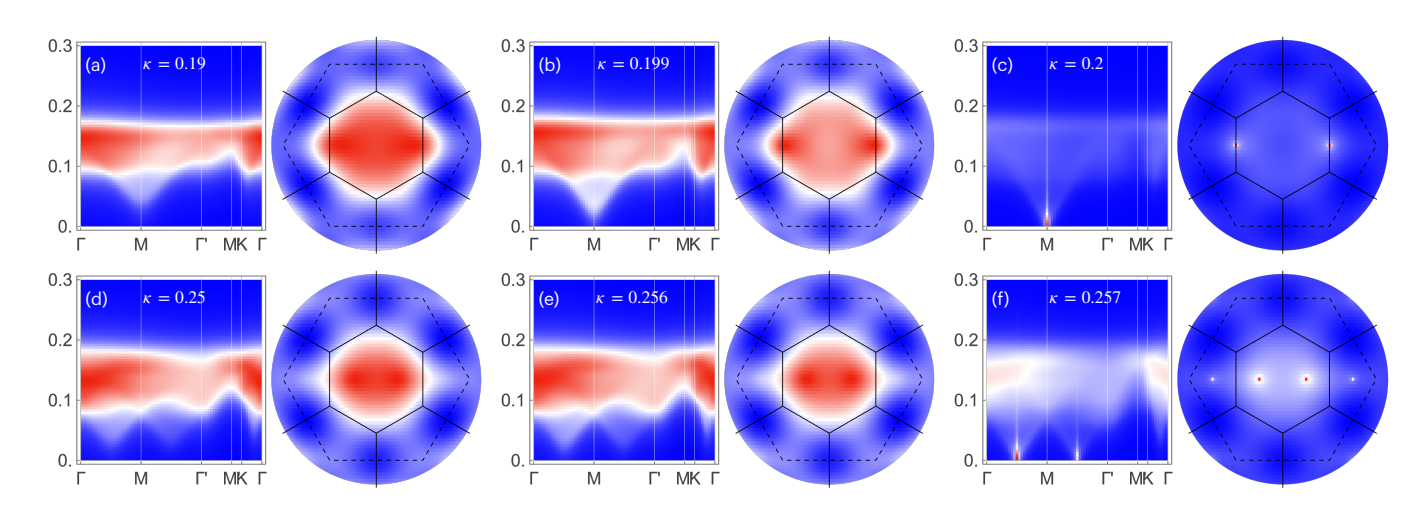


FIGURE 7. Dynamical and static spin-spin structure factors for the ZZ state (a,b,c) and the dZZ (d,e,f) state obtained within the g-SBMFT, for a system size of $8 \times 12 \times 12$ sites, at $J_3/|J_1| = 0.24$ and for various effective spin values $\kappa = 2S$, close to the Bose condensation points. The path for the dynamical structure factor is given in Fig. 1(c).

In Fig. 7, we present the dynamic and static structure factors for the ZZ and double dZZ obtained from the 8-site unit-cell g-SBMFT, evaluated for different values of the effective spin $\kappa=2S$, around the critical value at which each phase condenses.

Here we provide some elements about how the spin–spin correlation functions should be computed within SBMFT frameworks. It has recently been pointed out in the context of the Kitaev model [40] that the prescription adopted to evaluate $\langle \mathbf{S}_i \cdot \mathbf{S}_j \rangle$ can significantly affect the physical interpretation. In particular, one may either perform an explicit calculation of the Schwinger-boson operators in the bosonic vacuum, $\langle \hat{b}_i^{\dagger} \sigma^{\alpha} \hat{b}_i \hat{b}_j^{\dagger} \sigma^{\beta} \hat{b}_j \rangle$, as derived in Ref. [20], or use the same pairing/hopping decoupling employed to construct the mean-field theory, $\langle : \hat{h}^{\dagger} \hat{h} : -\hat{p}^{\dagger} \hat{p} \rangle$. Both of them are detailed in Appendix C under formalisms 1 and 2, respectively. Depending on the chosen prescription, important contributions to the correlations may be overlooked.

In our generalized g-SBMFT, it is not always possible to re-express teh spin correlations in terms of the operators, since nearest-neighbor (n.n.) and next-nearest-neighbor (n.n.n.) bonds are described by distinct sets of pairing and hopping operators. Consequently, there is no unique mean-field expression for the spin bilinears $\langle \mathbf{S}_i \cdot \mathbf{S}_j \rangle$

for any bond (i,j). A detailed comparison of both decoupling schemes is presented in Appendix D, where we demonstrate that the explicit evaluation of the bosonic operators in the vacuum ground state (with no Bogoliubov quasiparticles) systematically provides the most reliable results. Within s-SBMFT, both prescriptions yield identical results. However, for more complex Ansätze like those encountered in the g-SBMFT, the full vacuum evaluation is essential, as all relevant physical information is encoded in the saddle-point solution of the self-consistent equations. Accordingly, throughout this work we employ only the latter strategy, meaning that all real-space, static, and dynamical spin structure factors are computed from the full expectation value of the boson operators in the Bogoliubov vacuum representing the ground state.

As pointed out, within SBMFT, varying S in the mean-field calculation provides a convenient way to probe the stability of competing phases. We observe that the ZZ phase condenses more rapidly than the dZZ phase. However, in both cases, the critical condensation occurs at an effective spin value $S_c \simeq 0.1$, which implies that in a real spin- $\frac{1}{2}$ system, the corresponding magnetic order is even more robust and far from a possible quantum melting to their respective quantum spin liquids. Naturally, as already discussed above, describing such strongly developed magnetic orders within mean-field theory would

ultimately require the explicit inclusion of boson condensates and to exactly account for the boson constraint, a task that lies well beyond the scope of the present study.

Interestingly, the dynamical signatures of the two phases are found to be clearly distinct. When the system is in the disordered regime, i.e., for effective spin values below the critical threshold $(S < S_c)$ where quantum fluctuations dominate, precursor Goldstone modes emerge at the expected condensation points: at the M point of the BZ in the ZZ phase, and at M/2 in the dZZ phase. In the latter case, a striking feature is the stronger redistribution of spectral weight between the first and second BZs evident when comparing Fig. 7 (c) and (f), and that could be experimentally detected.

Experimentally, the relevant quantity is the neutronscattering intensity, which is proportional to the dynamical structure factor,

$$I(\mathbf{q},\omega) \propto \sum_{\alpha,\beta} \left(\delta_{\alpha\beta} - \frac{q_{\alpha}q_{\beta}}{|\mathbf{q}|^2} \right) S^{\alpha\beta}(\mathbf{q},\omega),$$
 (9)

where $S^{\alpha\beta}(\mathbf{q},\omega)$ is the spin-resolved dynamical structure factor defined in Eq. (8). Within our mean-field treatment, this expression makes explicit the redistribution of spectral weight across Brillouin zones, thus providing a direct experimental fingerprint of the difference between zig-zag and double zig-zag phases.

Such redistribution effects have already been hinted at in recent inelastic neutron scattering measurements on $BaCo_2(AsO_4)_2$, where intensity modulations between the first and second Brillouin zones were reported [5]. Our analysis provides a microscopic explanation of these observations, supporting the interpretation of $BaCo_2(AsO_4)_2$ as lying in close proximity to the double zig-zag regime.

The magnetic structure of $BaCo_2(AsO_4)_2$ has been unambiguously determined only recently through polarized neutron experiments [41] finding a nearly commensurate (0.27, 0, -1.31) dZZ phase. Note that the pure dZZ is described by the (0.25, 0, -1.31) wavevector. This order should display a Goldstone mode close to the M/2 point similar to the one in our Fig. 7 (f). This is in contrast with neutron scattering experiments which display a clear gap of magnitude, $\delta = 1.45$ meV at the Γ-point. The opening of a gap could be related to the presence of a gapped QSL as in our results of Fig. 7 (d), e). However, it would be inconsistent with the magnetic order observed. On the other hand, recent Monte Carlo simulations on a classical J-K- Γ - Γ' Kitaev-Heisenberg do find a the effective dZZ ground state i. e. with an incommensurate order (with wavevector (0.27, 0, -1.31) corresponding to defective uudd spin arrangement) consistent with observations. At the same time, the Monte Carlo simulations of the dynamical structure factor, $S(\mathbf{q}, \omega)$, are in excellent agreement with the magnetic excitation dispersions observed in INS experiments. These simulations are also able to describe the 1/3 plateau ascribed to the presence of uud spin order. In contrast, LSWT in periodic systems

would be unable to describe this state since it misses the incommensurability observed.

VI. CONCLUSIONS AND OUTLOOK

Motivated by the intriguing magnetic properties of $BaCo_2(AsO_4)_2$ (BCAO), we investigate the ferro-antiferromagnetic J_1 - J_3 Heisenberg model on the honeycomb lattice. To properly address the frustrated ferromagnetism intrinsic to this model, we develop a generalized Schwinger-boson mean-field theory (g-SBMFT) capable of treating ferromagnetic and antiferromagnetic interactions on an equal footing. In this framework, the set of mean-field parameters is enlarged to include both triplet pairing and singlet hopping channels, in addition to the conventional singlet pairing and triplet hopping terms already present in the standard s-SBMFT. This extension enables a unified description of competing exchange processes and allows us to derive the complete phase diagram of the J_1 – J_3 Heisenberg model, together with its dynamical magnetic properties directly relevant to experimental observations on BCAO.

Classically the model displays FM and ZZ phases at weak $J_3/|J_1|$ and large $J_3/|J_1|$, respectively, with an intermediate spiral phase arising in a small parameter region between them. Instead, our phase diagram displays an intermediate dZZ phase consistent with our ED calculations on small clusters and previous DMRG on finite cylinders (with 16² sites). Since our approach can reach, in practical terms, the thermodynamic limit (cluster sizes of 48²) it provides strong evidence of the existence of a dZZ phase in the J_1-J_3 model. The fact that this dZZ order is different from the intermediate spiral phase found classically indicates the prominent role of quantum fluctuations and an underlying order-from-disorder mechanism which stabilizes the dZZ phase. We note that the triplet pairing channels included in our approach are crucial for the stabilization of the dZZ phase. This avoids the difficulty of describing ferromagnetism in SBMFT at T=0 on arbitrarily large clusters without violating the boson number constraint [18].

We obtain the magnetic excitation spectra of the model in order to make contact with neutron scattering experiments. Above a critical $S > S_c \approx 0.1$ at which magnetic order sets in both the ZZ (dZZ) phase displays a minimum at the corresponding ordering wavevectors M(M/2) as expected from the Goldstone theorem. While the spectral weight is mostly concentrated on this wavevectors, for $S < S_c$ a gapped QSL occurs with a characteristic spectral weight redistribution over the 1st and 2nd BZs. In contrast, INS experiments on BCAO find a magnon dispersion which has a gap and a flat band minimum around the Γ -point resembling the excitation spectra of a 2D ferromagnet. This is inconsistent with elastic magnetic scattering experiments on BCAO which display incommensurate AFM order at sufficiently low T. Hence, there seems to be an inconsistency in experimental observations in BCAO between the static magnetic order observed and the absence of a Goldstone mode at the dZZ (or close to it) wavevector. A way out to this puzzle could be the effect of disorder, the fact that a dZZ is not perfectly formed but contains defects as recently pointed out [7]. These apparently contradictory phenomena may be explained from the proximity of BCAO to a FM instability. Experiments do find that even a tiny magnetic field along the b-direction can induce a FM transition. Thus, BCAO may be an example of a 2D quasi-FM ordered system on the verge of FM. However, these issues deserve further experimental analysis through next-generation INS and/or resonant X-ray scattering.

From the theoretical point of view, our work highlights g-SBMFT as a promising extension of SBMFT to investigate frustrated ferromagnets. It would be interesting to include the effect of an external magnetic field and explore the sensitivity of the dZZ to it. Other terms such as bond-dependent Kitaev terms and/or longer-range anisotropic interactions known to be relevant to BCAO as recently shown[6, 7] could, in principle, be included as further model refinements. The effect of disorder and/or lattice distortions on the delicate balance between ZZ, dZZ and FM phases relevant to BCAO deserve future work.

ACKNOWLEDGMENT

AR would like to thank Virginie Simonet and Armand Devillez for stimulating discussions. J. M. acknowledges financial support from (Grant No. PID2022-139995NB-I00) MICIN/FEDER, Unión Europea and from the María de Maeztu Programme for Units of Excellence in R&D (Grant No. CEX2023-001316-M)

Annexe A: Connection with standard SBMFT

This general theory can be easilly connected to the s-SBMFT formalism by imposing constraints on the structure of the mean-field parameters. For example, in the pairing basis $\hat{\mathbf{p}}_{ij} = (\hat{p}_{ij}^{\uparrow\uparrow}, \hat{p}_{ij}^{\downarrow\downarrow}, \hat{p}_{ij}^{\downarrow\uparrow}, \hat{p}_{ij}^{\downarrow\downarrow})$ and for an isotropic exchange coupling $\hat{J} = \operatorname{diag}(J^{xx}, J^{yy}, J^{zz})$ with $J^{xx} = J^{yy} = J^{zz} = J$, gives $\hat{\mathbf{S}}_i \hat{J} \hat{\mathbf{S}}_j = \frac{1}{4} \hat{\mathbf{p}}_{ij}^{\dagger} T \hat{\mathbf{p}}_{ij}$ with

$$\hat{T}_p = \begin{bmatrix} 1 & . & . \\ . & -1 & 2 & . \\ . & 2 & -1 & . \\ . & . & . & 1 \end{bmatrix}. \tag{A1}$$

If we now define the singlet operator

$$\hat{O}_A = \frac{1}{\sqrt{6}} \begin{bmatrix} \cdot & \cdot & \cdot & \cdot \\ \cdot & 1 & -1 & \cdot \\ \cdot & -1 & 1 & \cdot \\ \cdot & \cdot & \cdot & \cdot \end{bmatrix}, \tag{A2}$$

it is straightforward to verify that

$$\hat{A}^{\dagger}\hat{A} = -\frac{1}{4}\hat{\mathbf{p}}_{ij}^{\dagger}\hat{O}_{A}^{\dagger}\hat{T}_{p}\hat{O}_{A}\hat{\mathbf{p}}_{ij},\tag{A3}$$

with $\hat{A} = \frac{1}{2}(b_{i\uparrow}b_{j\downarrow} - b_{i\downarrow}b_{j\uparrow})$ the singlet pairing operator. In a similar way, the correspondence with the boson hopping $\hat{B} = \frac{1}{2}(b_{i\uparrow}^{\dagger}b_{j\uparrow} + b_{i\downarrow}^{\dagger}b_{j\downarrow})$ is given by

$$\hat{B}^{\dagger}\hat{B} = \frac{1}{4}\hat{\mathbf{h}}_{ij}^{\dagger}\hat{O}_{B}^{\dagger}\hat{T}_{h}\hat{O}_{B}\hat{\mathbf{h}}_{ij}, \tag{A4}$$

where we have used the hopping basis $\hat{\mathbf{h}}_{ij} = (\hat{h}_{ij}^{\uparrow\uparrow}, \hat{h}_{ij}^{\downarrow\downarrow}, \hat{h}_{ij}^{\downarrow\uparrow}, \hat{h}_{ij}^{\downarrow\downarrow})$ and defined the hopping operator and T tensor in this basis

$$\hat{O}_B = \frac{1}{\sqrt{6}} \begin{bmatrix} 1 & \dots & 1 \\ \dots & \dots & \dots \\ \dots & \dots & \dots \\ 1 & \dots & 1 \end{bmatrix}, \quad \hat{T}_h = \begin{bmatrix} 1 & \dots & 2 \\ \dots & -1 & \dots \\ \dots & \dots & -1 & \dots \\ 2 & \dots & \dots & 1 \end{bmatrix}. \quad (A5)$$

This concludes the connection with the standard SBMFT since we have established the well known relation $\hat{\mathbf{S}}_i\hat{\mathbf{S}}_j =: \hat{B}^{\dagger}\hat{B}: -\hat{A}^{\dagger}\hat{A}$ when the projections are used.

It is thus clear that depending the definition of the constraint pairing and hopping operators $\hat{O}_{p,h}$, any type of mean field can be constructed in a very flexible way.

Annexe B: Diagonalizing the SBMFT

We start by expressing the mean-field hamiltonian as:

$$H = \sum_{\mathbf{q}} \Psi^{\dagger} M_{\mathbf{q}} \Psi_{\mathbf{q}} + H' \tag{B1}$$

where : $\Psi_{\bf q} = (b^u_{{\bf q},\uparrow}b^v_{{\bf q},\uparrow}b^{u\dagger}_{-{\bf q},\downarrow}b^{v\dagger}_{-{\bf q},\downarrow})^T$ and $M_{\bf q}$ a 4 × 4 matrix. The hamiltonian can be diagonalized through the transformation $\Psi_{\bf q} = P_{\bf q}\Gamma_{\bf q}$:

$$H = \sum_{\mathbf{q}} \Gamma_{\mathbf{q}}^{\dagger} M_{\mathbf{q}} \Gamma_{\mathbf{q}} + H'$$
 (B2)

where $\Gamma_{\mathbf{q}} = (\gamma_{\mathbf{q},\uparrow}^1 \gamma_{\mathbf{q},\uparrow}^2 \gamma_{-\mathbf{q},\downarrow}^{1\dagger} \gamma_{-\mathbf{q},\downarrow}^{2\dagger})^T$ which satisfies the two conditions :

$$P_{\mathbf{q}}^{\dagger} M_{\mathbf{q}} P_{\mathbf{q}} = \omega_{\mathbf{q}}$$

$$P_{\mathbf{q}}^{\dagger} \tau^{z} P_{\mathbf{q}} = \tau^{z}$$
(B3)

where $\omega_{\mathbf{q}} = diag(\omega_1, \omega_2, \omega_1, \omega_2)$ is a diagonal matrix containing the bosonic eigen-frequencies and $\tau^z = diag(1,1,-1,-1)$. This is equivalent to the generalized eigenvalue problem : $\tau^z M_{\mathbf{q}} P_{\mathbf{q}} = P_{\mathbf{q}} \tau^z \omega_{\mathbf{q}}$. Thus, the transformation matrix $T_{\mathbf{q}}$ that satisfies the above two conditions simultaneously contains the eigenvectors of $\sigma^z M_{\mathbf{q}}$ in its columns and $\tau^z \omega_{\mathbf{q}}$ contains the bosonic eigen-frequencies in pairs $(\omega_\mu, -\omega_\mu)$ with $\omega_\mu > 0$. After the numerical diagonalization of $\tau^z M_{\mathbf{q}}$, the eigenvectors, ω_ρ , should be para-normalized so that they satisfy : $\omega_\rho^\dagger \tau^z \omega_\rho' = [\tau^z]_{\rho \rho'}$.

Annexe C: Spin correlation calculations

In this appendix, we present two possible approaches to calculate the spin-spin correlations in the SBMFT. The first one is the direct and general calculation of the expectation values of the four boson operators in the mean-field vacuum. The second is based on the re-expression of the spin bilinears in function of the pairing and hopping operators as used in the mean-field decoupling of the hamiltonian.

Formalism 1: Full vacuum calculation.

Following the general formulation of the spin structure factors [42], we can derive the most general expression for our present four-boson generalized SBMFT. By definition the spin correlation between the component α on a reference site $\mathbf{r}_0 + \mathbf{d}_u$ and β on site $\mathbf{r}_j + \mathbf{d}_v$, where \mathbf{d}_u is the sub-lattice vector, is given by

$$\langle S_{\mathbf{r}_{0}+\mathbf{d}_{u}}^{\alpha} S_{\mathbf{r}_{j}+\mathbf{d}_{v}}^{\beta} \rangle = \frac{1}{n_{c}} \sum_{i} \langle S_{\mathbf{r}_{i}+\mathbf{d}_{u}}^{\alpha} S_{\mathbf{r}_{i}+\mathbf{d}_{u}+\mathbf{r}_{j}+\mathbf{d}_{v}}^{\beta} \rangle \quad (C1)$$
$$= \frac{1}{n_{c}} \sum_{i} M_{\sigma_{0}\sigma_{1}\sigma_{2}\sigma_{3}}^{\alpha\beta} \langle b_{i,\sigma_{0}}^{u+} b_{i,\sigma_{1}}^{u} b_{j,\sigma_{2}}^{v+} b_{j,\sigma_{3}}^{v} \rangle$$

where translational invariance has been used and with $M_{\sigma_0\sigma_1\sigma_2\sigma_3}^{\alpha\beta} = \sigma_{s_0s_1}^{\alpha} \otimes \sigma_{\sigma_2\sigma_3}^{\beta}$ a 4 × 4 matrix defined from the Pauli matrices. Note that implicit summation is used for repeated spin indices σ_i .

Performing the Fourier transform on the bosonic operators

$$b_{i,\sigma}^{u} = \frac{1}{\sqrt{n_c}} \sum_{\mathbf{q}} e^{i\mathbf{q}\cdot(\mathbf{r}_i + \mathbf{d}_u)} b_{\mathbf{q},\sigma}^{u}, \tag{C2}$$

one can recast the correlation as

$$\begin{split} \langle S^{\alpha}_{\mathbf{r}_{0}+\mathbf{d}_{u}} S^{\beta}_{\mathbf{r}_{j}+\mathbf{d}_{v}} \rangle \; &= \; \frac{1}{n_{c}^{2}} M^{\alpha\beta}_{\sigma_{0}\sigma_{1}\sigma_{2}\sigma_{3}} \sum_{\mathbf{q}_{0},\mathbf{q}_{1},\mathbf{q}_{2}} e^{i(\mathbf{q}_{0}-\mathbf{q}_{1})\cdot(\mathbf{r}_{j}+\mathbf{d}_{v}-\mathbf{d}_{u})} \langle b^{u+}_{\mathbf{q}_{0},\sigma_{0}} b^{u}_{\mathbf{q}_{1},\sigma_{1}} b^{v+}_{\mathbf{q}_{2},\sigma_{2}} b^{v}_{\mathbf{q}_{3},\sigma_{3}} \rangle \\ &= \; \frac{1}{n_{c}^{2}} M^{\alpha\beta}_{\sigma_{0}\sigma_{1}\sigma_{2}\sigma_{3}} \sum_{\mathbf{q}_{0},\mathbf{q}_{1},\mathbf{q}_{2}} e^{i(\mathbf{q}_{0}-\mathbf{q}_{1})\cdot(\mathbf{r}_{j}+\mathbf{d}_{v}-\mathbf{d}_{u})} \\ &\times \; \sum_{\{l\}} \sum_{\{\sigma_{l}\}} P^{(-\mathbf{q}_{0})}_{(u,\sigma_{0},1),(r,\sigma_{r},0)} P^{(\mathbf{q}_{1})}_{(u,\sigma_{1},0),(s,\sigma_{s},0)} P^{(-\mathbf{q}_{2})}_{(v,\sigma_{2},1),(m,\sigma_{m},1)} P^{(\mathbf{q}_{3})}_{(v,\sigma_{3},0),(n,\sigma_{n},1)} \langle \gamma^{r}_{-\mathbf{q}_{0},\sigma_{r}} \gamma^{s}_{\mathbf{q}_{1},\sigma_{s}} \gamma^{m+}_{\mathbf{q}_{2},\sigma_{m}} \gamma^{n+}_{-\mathbf{q}_{3},\sigma_{n}} \rangle \\ &+ \; \frac{1}{N_{c}^{2}} M^{\alpha\beta}_{\sigma_{0}\sigma_{1}\sigma_{2}\sigma_{3}} \sum_{\mathbf{q}_{0},\mathbf{q}_{1},\mathbf{q}_{2}} e^{i(\mathbf{q}_{0}-\mathbf{q}_{1})\cdot(\mathbf{r}_{j}+\mathbf{d}_{v}-\mathbf{d}_{u})} \\ &\times \; \sum_{\{l\}} \sum_{\{\sigma_{l}\}} P^{(-\mathbf{q}_{0})}_{(u,\sigma_{0},1),(r,\sigma_{r},0)} P^{(\mathbf{q}_{1})}_{(u,\sigma_{1},0),(s,\sigma_{s},1)} P^{(-\mathbf{q}_{2})}_{(v,\sigma_{2},1),(m,\sigma_{m},0)} P^{(\mathbf{q}_{3})}_{(v,\sigma_{3},0),(n,\sigma_{n},1)} \langle \gamma^{r}_{-\mathbf{q}_{0},\sigma_{r}} \gamma^{s+}_{-\mathbf{q}_{1},\sigma_{s}} \gamma^{m}_{-\mathbf{q}_{2},\sigma_{m}} \gamma^{n+}_{-\mathbf{q}_{3},\sigma_{n}} \rangle \end{split}$$

where $\mathbf{q}_3 = \mathbf{q}_2 + \mathbf{q}_0 - \mathbf{q}_1$, $\{l\} = (r, s, m, n)$, $\{\sigma_l\} = (\sigma_r, \sigma_s, \sigma_m, \sigma_n)$, and where we have reexpressed the operators in terms of the eigenmodes:

$$\begin{bmatrix} b_{\mathbf{q},\sigma}^{u} \\ b_{-\mathbf{q},\sigma}^{u+} \end{bmatrix} = P^{(\mathbf{q})} \begin{bmatrix} \gamma_{\mathbf{q},\sigma_{r}}^{r} \\ \gamma_{-\mathbf{q},\sigma_{r}}^{r+} \end{bmatrix}. \tag{C3}$$

In this notation, an element of the eigen-matrix is given by $P_{(u,\sigma_u,a),(v,\sigma_v,b)}^{(\mathbf{q})}$ with a and b=0 or 1 depending on whether we consider annihilation operators ordered in the first $2n_u$ elements, or creation ones in the last $2n_u$.

From the above equations, only three contractions give

non-zero expectation values:

$$C_1: \quad \mathbf{q}_2 = -\mathbf{q}_0, \quad r = m, \quad \sigma_r = \sigma_m, \quad (C4)$$

$$\mathbf{q}_3 = -\mathbf{q}_1, \quad s = n, \quad \sigma_s = \sigma_n,$$

$$C_2:$$
 $\mathbf{q}_2 = \mathbf{q}_1, \quad s = m, \quad \sigma_s = \sigma_m,$ (C5)
 $\mathbf{q}_3 = \mathbf{q}_0, \quad r = n, \quad \sigma_r = \sigma_n,$

$$C_3:$$
 $\mathbf{q}_0 = \mathbf{q}_1, \quad s = m, \quad \sigma_s = \sigma_m,$ (C6)
 $\mathbf{q}_2 = \mathbf{q}_3, \quad r = n, \quad \sigma_r = \sigma_n.$

Finally, noting that $P_{(u,\sigma_u,a),(v,\sigma_v,b)}^{(-\mathbf{q})} = \bar{P}_{(u,\sigma_u,\bar{a}),(v,\sigma_v,\bar{b})}^{(\mathbf{q})}$, where we have defined $\bar{a} = (1,0)$ if a = (0,1). we arrive to the final general expression

$$\begin{split} \langle S_{r_0+\delta_u}^{\alpha} S_{r_j+\delta_v}^{\beta} \rangle &= \frac{1}{n_c^2} M_{\sigma_0\sigma_1\sigma_2\sigma_3}^{\alpha\beta} \sum_{\mathbf{q}_0,\mathbf{q}_1} e^{i(\mathbf{q}_0-\mathbf{q}_1)\cdot(\mathbf{r}_j+\mathbf{d}_v-\mathbf{d}_u)} \\ &\times \sum_{r,s} \sum_{\sigma_r,\sigma_s} \bar{P}_{(u,\sigma_0,0),(r,\sigma_r,1)}^{(\mathbf{q}_0)} P_{(u,\sigma_1,0),(s,\sigma_s,0)}^{(\mathbf{q}_1)} P_{(v,\sigma_2,1),(r,\sigma_r,1)}^{(\mathbf{q}_0)} \bar{P}_{(v,\sigma_3,1),(s,\sigma_s,0)}^{(\mathbf{q}_1)} \\ &+ \frac{1}{n_c^2} M_{\sigma_0\sigma_1\sigma_2\sigma_3}^{\alpha\beta} \sum_{\mathbf{q}_0,\mathbf{q}_1} e^{i(\mathbf{q}_0-\mathbf{q}_1)\cdot(\mathbf{r}_j+\mathbf{d}_v-\mathbf{d}_u)} \\ &\times \sum_{r,s} \sum_{\sigma_r,\sigma_s} \bar{P}_{(u,\sigma_0,0),(r,\sigma_r,1)}^{(\mathbf{q}_0)} P_{(u,\sigma_1,0),(s,\sigma_s,0)}^{(\mathbf{q}_1)} \bar{P}_{(v,\sigma_2,0),(s,\sigma_s,0)}^{(\mathbf{q}_0)} P_{(v,\sigma_3,0),(r,\sigma_r,1)}^{(\mathbf{q}_0)} \\ &+ \frac{1}{n_c^2} M_{\sigma_0\sigma_1\sigma_2\sigma_3}^{\alpha\beta} \sum_{\mathbf{q}_0,\mathbf{q}_1} \sum_{r,s} \sum_{\sigma_r,\sigma_s} \bar{P}_{(u,\sigma_0,0),(r,\sigma_r,1)}^{(\mathbf{q}_0)} P_{(u,\sigma_1,0),(r,\sigma_r,1)}^{(\mathbf{q}_0)} \bar{P}_{(v,\sigma_2,0),(s,\sigma_s,1)}^{(\mathbf{q}_0)} P_{(v,\sigma_3,0),(r,\sigma_r,1)}^{(\mathbf{q}_1)} \end{split}$$

When the system has no condensate (is gapped), the contraction C_3 is zero since it corresponds to onsite expectation values, namely the spin value at site $\mathbf{r}_i + \mathbf{d}_u$. It has been displayed for completeness of the general formulation.

Formalism 2: Re-expression in terms of operators.

For completeness, we provide details about the calcu-

lation of the spin correlations in real space obtained from s-SBMFT which can be found elsewhere [17, 27, 43, 44]. Once the eigenvalues and eigenvectors are obtained one can evaluate the spin correlations:

$$\langle \mathbf{S}_{\mathbf{r}_i + \delta_u} \cdot \mathbf{S}_{\mathbf{r}_j + \mathbf{d}_v} \rangle = |B_{ij}^{uv}|^2 - |A_{ij}^{uv}|^2. \tag{C7}$$

After Fourier transforming the boson operators using Eq. (C2), the variational parameters are reexpressed as:

$$\begin{split} A^{uv}_{ij} &= \frac{1}{2} (\langle b^u_{i\uparrow} b^v_{j\downarrow} \rangle - \langle b^u_{i\downarrow} b^v_{j\uparrow} \rangle) = \frac{1}{2n_c} \sum_{\mathbf{q}} \left(e^{i\mathbf{q}\cdot(\mathbf{r}_i + \mathbf{d}_u - \mathbf{r}_j - \mathbf{d}_v)} \langle b^u_{\mathbf{q}\uparrow} b^v_{-\mathbf{q}\downarrow} \rangle - e^{-i\mathbf{q}\cdot(\mathbf{r}_i + \mathbf{d}_u - \mathbf{r}_j - \mathbf{d}_v)} \langle b^u_{-\mathbf{q}\downarrow} b^v_{\mathbf{q}\uparrow} \rangle \right), \\ B^{uv}_{ij} &= \frac{1}{2} (\langle b^{u\dagger}_{i\uparrow} b^v_{j\uparrow} \rangle + \langle b^{u\dagger}_{i\downarrow} b^v_{j\downarrow} \rangle) = \frac{1}{2n_c} \sum_{\mathbf{q}} \left(e^{-i\mathbf{q}\cdot(\mathbf{r}_i + \mathbf{d}_u - \mathbf{r}_j - \mathbf{d}_v)} \langle b^{u\dagger}_{\mathbf{k}\uparrow} b^v_{\mathbf{q}\uparrow} \rangle + e^{i\mathbf{q}\cdot(\mathbf{r}_i + \mathbf{d}_u - \mathbf{r}_j - \mathbf{d}_v)} \langle b^{\dagger u}_{-\mathbf{k}\downarrow} b^v_{-\mathbf{q}\downarrow} \rangle \right). \end{split}$$

The mean-field averages may be evaluated from the

transformation $\Psi_{\mathbf{q}} = P^{(\mathbf{q})}\Gamma_{\mathbf{q}}$ with:

$$P^{(\mathbf{q})} = \begin{bmatrix} U_{\mathbf{q}} & X_{\mathbf{q}} \\ V_{\mathbf{q}} & Y_{\mathbf{q}} \end{bmatrix}, \tag{C8}$$

where the 4×4 $T_{\bf q}$ matrix has been divided into 2×2 submatrices. Using the fact that the ground state of the system is the vacuum of Bogoliubov excitations: $\gamma_{{\bf q}\sigma}|\Omega\rangle=0$,

$$\begin{split} A^{uv}_{ij} &= \frac{1}{2n_c} \sum_{\mathbf{q}} \left(e^{i\mathbf{q}\cdot(\mathbf{r}_i + \mathbf{d}_u - \mathbf{r}_j - \mathbf{d}_v)} \sum_{w} [U_{\mathbf{q}}]_{uw} [V_{\mathbf{q}}]_{vw}^* - e^{-i\mathbf{q}\cdot(\mathbf{r}_i + \mathbf{d}_u - \mathbf{r}_j - \mathbf{d}_v)} \sum_{w} [Y_{\mathbf{q}}]_{uw}^* [X_{\mathbf{q}}]_{vw} \right) \\ B^{uv}_{ij} &= \frac{1}{2n_c} \sum_{\mathbf{q}} \left(e^{-i\mathbf{q}\cdot(\mathbf{r}_i + \mathbf{d}_u - \mathbf{r}_j - \mathbf{d}_v)} \sum_{w} [X_{\mathbf{q}}]_{uw}^* [X_{\mathbf{q}}]_{vw} + e^{i\mathbf{q}\cdot(\mathbf{r}_i + \mathbf{d}_u - \mathbf{r}_j - \mathbf{d}_v)} \sum_{w} [V_{\mathbf{q}}]_{uw} [V_{\mathbf{q}}]_{vw}^* \right), \end{split}$$

from which $\langle \mathbf{S}_{\mathbf{r}_i + \mathbf{d}_u} \cdot \mathbf{S}_{\mathbf{r}_j + \mathbf{d}_v} \rangle$ can be evaluated through Eq. C7 and plotted in Fig. 6 of the main text.

Annexe D: Comparison of the spin correlation formalisms

As recently discussed by Sasamoto and Nasu [40], there exists several possible prescriptions for evaluating

spin correlations within the SBMFT framework, as detailed in the preceding Appendices. Their analysis of the Kitaev model demonstrated that the two common approaches—detailed in Appendix C-can yield different results, and that important physical features may be missed if the choice of prescription is not treated carefully. In the present work, we show that, as expected, the most general and reliable formulation is that based on the explicit evaluation of the bosonic operators in the full vacuum, as developed in Ref. [20]. This approach remains valid regardless of the specific mean-field decoupling chosen for the Hamiltonian. It is particularly relevant in our case, where ferromagnetic and antiferromagnetic bonds are described using distinct pairing and hopping opera-

tors, making the simpler operator-based inapplicable due to the absence of a unique definition for spin bilinears $\langle S_i S_j \rangle$ consistent with any bond (i,j). To enable a direct comparison between the two schemes, we first performed a systematic and exact evaluation of the four-boson operators in the bosonic vacuum as described in Appendix C. In parallel, we examined three distinct mean-field decouplings of the Hamiltonian, each based on different combinations of pairing and hopping operators. For example, the first one corresponds to the one detailed in Appendix C. The three different types of decoupling are displayed in the three lines of Fig. 8, and where each column corresponds to respectively the ZZ phase obtained within the s-SBMFT, the ZZ phase obtained by the g-SBMFT and the dZZ phase.

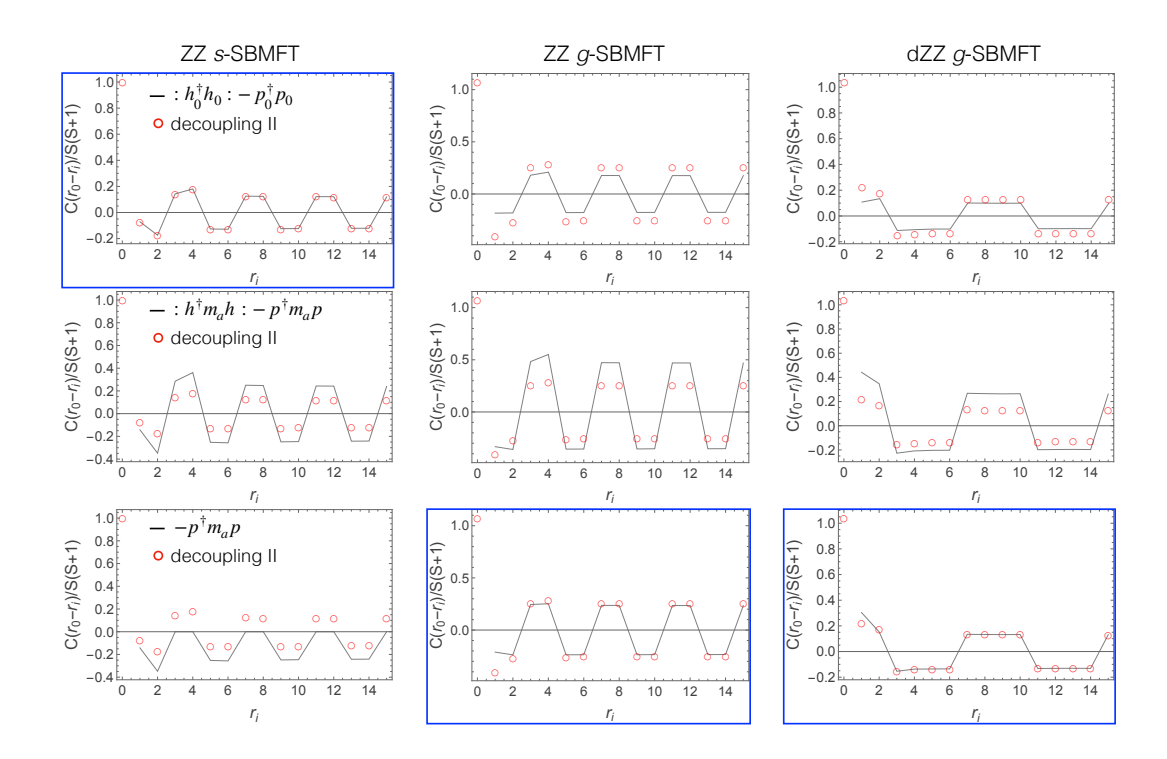


FIGURE 8. Comparison of real-space spin correlations computed using the full expectation value in the bosonic vacuum (red symbols), corresponding to decoupling I, with three different decoupling II schemes: (i) the standard h_0/p_0 formulation, (ii) a generalized hopping/pairing SBMFT, and (iii) the pairing-only case with $m_0 = (1, -1/3, -1/3, -1/3)$ as defined in Ref. [39]. For each Ansatz, a blue box highlights the case where the two decoupling schemes yield equivalent results.

This systematic comparison highlights that the full vacuum calculation consistently yields the most symmetric spin correlations, where the amplitudes of up- and downspin components are equal, as expected for perfectly ordered phases such as ZZ and dZZ. In the case of the conventional s-SBMFT, where all bonds in the Hamiltonian are expressed in terms of singlet pairing and spi-

non hopping operators, the two decoupling schemes are found to be strictly equivalent. Consequently, the general vacuum formulation (decoupling I), which makes no additional assumptions, provides the correct physical result in this limit.

In contrast, within the generalized g-SBMFT, where nearest-neighbor and next-nearest-neighbor bonds are

treated using distinct operators due to their ferromagnetic or antiferromagnetic character, the operator-based decoupling of the Hamiltonian cannot be applied uniformly to all pairs of sites. Depending on the specific operator construction, the two decoupling schemes may yield clearly different results. For both the ZZ and dZZ phases obtained from the g-SBMFT, we have nevertheless identified the appropriate operator formulation that reproduces the results of decoupling I at sufficiently large distances from the reference site. Interestingly, this correct formulation corresponds to the SBMFT construction introduced in Ref. [39], in which the spin bilinear

$$\mathbf{S}_i \cdot \mathbf{S}_j = \sum_{\alpha=1}^3 S_i^{\alpha} S_j^{\alpha}$$

is naturally satisfied without imposing any additional relations. We note that this is not the case in the formulation of Ref. [40], which may explain the appearance of spurious spectral weight in their calculated dynamical structure factor.

To conclude this systematic comparison study, we also have compared component by component of the spin correlations in the most complex Ansatz of our present work, the dZZ phase. This is displayed in Fig. 9 for (i) the full vacuum expectation calculation (red symbols) and (ii) the explicit mean-field decoupling in the real-space bosons corresponding to Eq. 45 of [40] (gray lines).

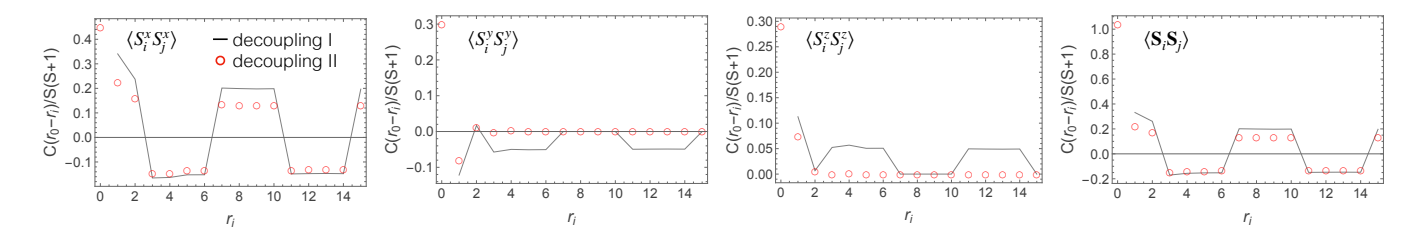


FIGURE 9. Comparison of real-space spin correlations computed from the full expectation value in the bosonic vacuum (red symbols), corresponding to decoupling, and from the real-space decoupling of the bosons [see Eq. (45) of Ref. [40]]. From left to right, individual spin-spin components are shown, followed by the total spin correlation.

This figure clearly demonstrates that the real-space decoupling and the full vacuum calculation yield markedly different results for the three spin components. In particular, the y and z components vanish identically in the latter case, indicating that the underlying Ansatz corresponds to spins aligned along the x direction. When the three components are summed, the operator-based calculation produces symmetric oscillations of the up- and down-spin correlations, whereas the real-space decoupling artificially favors one spin component. These results confirm that the general, unbiased, and assumption-free evaluation of correlations in the bosonic vacuum should be preferred to any alternative decoupling scheme, as it avoids subtle artifacts and unphysical asymmetries. ,,

Annexe E: dZZ order from exact diagonalization

In order to analyze the possible different magnetic orders in the J_1 - J_3 Heisenberg model on the honeycomb lattice we have performed ED calculations on the 24-site (8×3) cluster of Fig. 10 (c).

The behavior of the static spin structure factor, $S(\mathbf{q})$, across the FM to ZZ transition is shown in Fig. 10. While for $J_3 < 0.23$ a large peak at the Γ -point signaling the presence of FM order occurs, for $J_3 > 0.26$ a peak at the M-point associated with ZZ-order dominates $S(\mathbf{q})$. This is consistent with the FM state expected for $J_3 \to 0$ and the ZZ order at large J_3 . Strikingly, in the intermediate region $J_3 \approx 0.23 - 0.25$ a peak at the M/2-point corresponding to dZZ order emerges dominating $S(\mathbf{q})$.

Our results are consistent with previous DMRG calculations on large cylinders [14] with a similar cluster structure which have also found a small intermediate region where the dZZ state is stable. This also supports our SBMFT analysis in the main text. On the other hand, $S(\mathbf{q})$ on the fully symmetric hexagonal 24-site cluster shown in Fig. 10 (c) does not add useful information on the dZZ order since it misses the M/2-point.

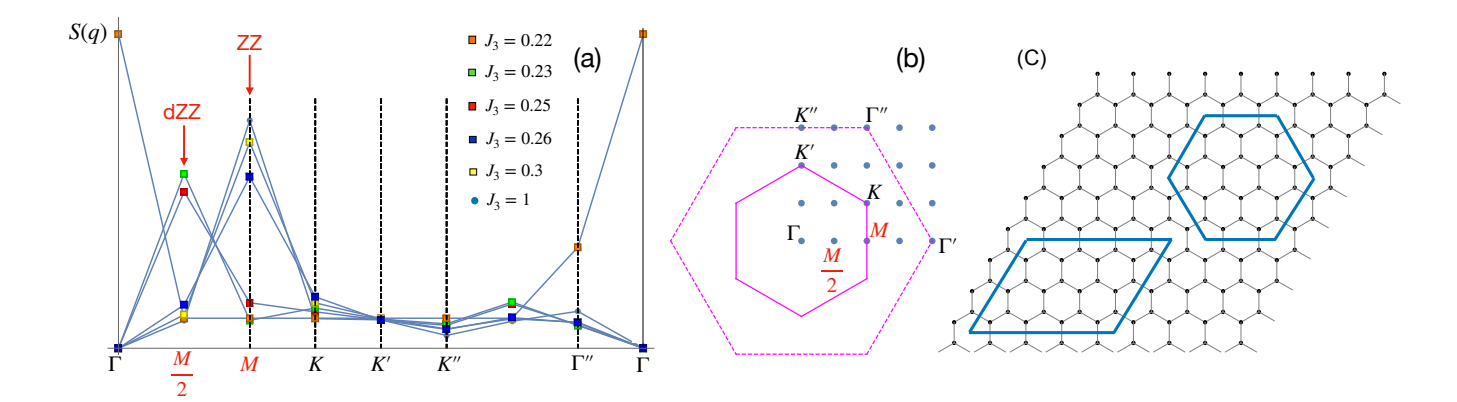


FIGURE 10. Static spin structure factor from ED of the J_1-J_3 model on the honeycomb lattice. In (a) the static spin structure factor for increasing J_3 is plotted along a path: $\Gamma-M-K-K'-K''-\Gamma''$ picking several symmetry points displayed in (b). The relevant $M=(2\pi/\sqrt{3},0)$ and M/2 wavevectors corresponding to the relevant ZZ and dZZ magnetic orders are marked in red for clarity. The vertical dashed black lines mark the symmetry points. The solid (dashed) pink lines denote the 1st (2nd) BZs of the honeycomb lattice and the blue circles in (b) are the allowed wavevectors for the 8×3 cluster with PBC shown in (c). (c) The two 24-site clusters with different shapes and PBC used for the calculations: the 8×3 (lower left), and the hexagonal fully symmetric (upper right).

- J. Chaloupka, G. Jackeli, and G. Khaliullin, Kitaev-Heisenberg Model on a Honeycomb Lattice: Possible Exotic Phases in Iridium Oxides A 2 IrO 3, Physical Review Letters 105, 027204 (2010).
- [2] S. Sinn, C. H. Kim, B. H. Kim, K. D. Lee, C. J. Won, J. S. Oh, M. Han, Y. J. Chang, N. Hur, H. Sato, B.-G. Park, C. Kim, H.-D. Kim, and T. W. Noh, Electronic Structure of the Kitaev Material α-RuCl₃ Probed by Photoemission and Inverse Photoemission Spectroscopies, Scientific Reports 6, 39544 (2016).
- [3] T. Yokoi, S. Ma, Y. Kasahara, S. Kasahara, T. Shibauchi, N. Kurita, H. Tanaka, J. Nasu, Y. Motome, C. Hickey, S. Trebst, and Y. Matsuda, Half-integer quantized anomalous thermal Hall effect in the Kitaev material candidate α -RuCl ₃, Science **373**, 568 (2021).
- [4] Y. Kasahara, T. Ohnishi, Y. Mizukami, O. Tanaka, S. Ma, K. Sugii, N. Kurita, H. Tanaka, J. Nasu, Y. Motome, T. Shibauchi, and Y. Matsuda, Majorana quantization and half-integer thermal quantum Hall effect in a Kitaev spin liquid, Nature 559, 227 (2018).
- [5] M. Songvilay, J. Robert, S. Petit, J. A. Rodriguez-Rivera, W. D. Ratcliff, F. Damay, V. Balédent, M. Jiménez-Ruiz, P. Lejay, E. Pachoud, A. Hadj-Azzem, V. Simonet, and C. Stock, Kitaev interactions in the co honeycomb antiferromagnets Na₃Co₂SbO₆ and Na₂Co₂TeO₆, Physical Review B 102, 224429 (2020).
- [6] P. A. Maksimov, S. Jiang, L. P. Regnault, and A. L. Chernyshev, Strong kitaev interaction in baco₂(aso₄)₂, Phys. Rev. Lett. 135, 066703 (2025).
- [7] A. Devillez, J. Robert, E. Lhotel, R. Ballou, C. Cavenel, F. D. Romero, Q. Faure, H. Jacobsen, J. Lass, D. G. Mazzone, U. B. Hansen, M. Enderle, S. Raymond, S. D. Brion, V. Simonet, and M. Songvilay, Bond-dependent interactions and ill-ordered state in the honeycomb co-baltate baco₂(aso₄)₂, arXiv:2503.22300 (2025).

- [8] L. P. Regnault and J. Rossat-Mignod, Phase transitions in quasi two-dimensional planar magnets (Springer Netherlands, 1990).
- [9] P. A. Maksimov, A. V. Ushakov, Z. V. Pchelkina, Y. Li, S. M. Winter, and S. V. Streltsov, Ab initio guided minimal model for the kitaev material BaCo₂(AsO₄)₂: Importance of direct hopping, third-neighbor exchange, and quantum fluctuations, Physical Review B 106, 165131 (2022).
- [10] P. A. Maksimov, Proximity-induced sequence of field transitions in the kitaev candidate BaCo₂(AsO₄)₂, Physical Review B 108, L180405 (2023).
- [11] X. Liu and H.-Y. Kee, Non-kitaev versus kitaev honeycomb cobaltates, Physical Review B 107, 054420 (2023).
- [12] S. Lee, S. Zhang, S. M. Thomas, L. Pressley, C. A. Bridges, E. S. Choi, V. S. Zapf, S. M. Winter, and M. Lee, Quantum order by disorder is a key to understanding the magnetic phases of BaCo₂AsO₄)₂, npj Quantum Materials 10, 11 (2025).
- [13] S. Das, S. Voleti, T. Saha-Dasgupta, and A. Parame-kanti, Xy magnetism, kitaev exchange, and long-range frustration in the $J_{\rm eff}=\frac{1}{2}$ honeycomb cobaltates, Physical Review B **104**, 134425 (2021).
- [14] S. Jiang, S. R. White, and A. L. Chernyshev, Quantum phases in the honeycomb-lattice J_1 – J_3 ferroantiferromagnetic model, Physical Review B **108**, L180406 (2023).
- [15] A. Auerbach, Interacting electrons and quantum magnetism (Springer New York, NY, 2012).
- [16] D. P. Arovas and A. Auerbach, Functional integral theories of low-dimensional quantum heisenberg models, Physical Review B 38, 316 (1988).
- [17] S. Sachdev, Kagomé- and triangular-lattice heisenberg antiferromagnets: Ordering from quantum fluctuations and quantum-disordered ground states with unconfined

- bosonic spinons, Physical Review B 45, 12377 (1992).
- [18] H. Feldner, D. C. Cabra, and G. L. Rossini, Ferromagnetic frustrated spin systems on the square lattice: Schwinger boson study, Physical Review B 84, 214406 (2011), arXiv: 1106.5018.
- [19] T. Lugan, L. D. C. Jaubert, M. Udagawa, and A. Ralko, Schwinger boson theory of the $J_1, J_2 = J_3$ kagome antiferromagnet, Physical Review B **106**, L140404 (2022).
- [20] J. C. Halimeh and M. Punk, Spin structure factors of chiral quantum spin liquids on the kagome lattice, Physical Review B 94, 104413 (2016).
- [21] P. Kos and M. Punk, Quantum spin liquid ground states of the heisenberg-kitaev model on the triangular lattice, Physical Review B 95, 024421 (2017).
- [22] B. Schneider, J. C. Halimeh, and M. Punk, Projective symmetry group classification of chiral F_2 spin liquids on the pyrochlore lattice: Application to the spin- $\frac{1}{2}$ xxz heisenberg model, Physical Review B 105, 125122 (2022).
- [23] M. Kargarian, A. Langari, and G. A. Fiete, Unusual magnetic phases in the strong interaction limit of two-dimensional topological band insulators in transition metal oxides, Physical Review B 86, 205124 (2012).
- [24] X. Yang and F. Wang, Schwinger boson spin-liquid states on square lattice, Phys. Rev. B 94, 035160 (2016).
- [25] F. Wang and A. Vishwanath, Spin-liquid states on the triangular and kagomé lattices: A projective-symmetrygroup analysis of schwinger boson states, Phys. Rev. B 74, 174423 (2006).
- [26] F. Wang, Schwinger boson mean field theories of spin liquid states on a honeycomb lattice: Projective symmetry group analysis and critical field theory, Phys. Rev. B 82, 024419 (2010).
- [27] J. Merino and A. Ralko, Role of quantum fluctuations on spin liquids and ordered phases in the heisenberg model on the honeycomb lattice, Physical Review B 97, 205112 (2018).
- [28] S. Sarker, C. Jayaprakash, H. R. Krishnamurthy, and M. Ma, Bosonic mean-field theory of quantum Heisenberg spin systems: Bose condensation and magnetic order, Physical Review B 40, 5028 (1989).
- [29] C. Wu, B. Chen, X. Dai, Y. Yu, and Z.-B. Su, Schwinger-boson mean-field theory of the heisenberg ferrimagnetic spin chain, Physical Review B 60, 1057 (1999).
- [30] S.-S. Zhang, E. A. Ghioldi, L. O. Manuel, A. E. Trumper, and C. D. Batista, Schwinger boson theory of ordered magnets, Physical Review B 105, 224404 (2022).
- [31] X. Yan, Z.-G. Zhu, and G. Su, Combined study of Schwinger-boson mean-field theory and linearized tensor renormalization group on Heisenberg ferromagnetic mixed spin (S, σ) chains, AIP Advances 5, 077183

- (2015).
- [32] A. E. Trumper, L. O. Manuel, C. J. Gazza, and H. A. Ceccatto, Schwinger-Boson Approach to Quantum Spin Systems: Gaussian Fluctuations in the "Natural" Gauge, Physical Review Letters 78, 2216 (1997).
- [33] T. Tay and O. I. Motrunich, Variational study of J_1 - J_2 heisenberg model on kagome lattice using projected schwinger-boson wave functions, Physical Review B (2011).
- [34] F. Wang and R. Tao, Schwinger-boson approach to the two-dimensional antiferromagnetic heisenberg model beyond the mean-field approximation, Physical Review B 61, 3508 (2000).
- [35] L. O. Manuel, C. J. Gazza, A. E. Trumper, and H. A. Ceccatto, Heisenberg model with Dzyaloshinskii-Moriya interaction: A mean-field Schwinger-boson study, Physical Review B 54, 12946 (1996).
- [36] L. Messio, O. Cépas, and C. Lhuillier, Schwingerboson approach to the kagome antiferromagnet with dzyaloshinskii-moriya interactions: Phase diagram and dynamical structure factors, Physical Review B 81, 064428 (2010).
- [37] L. Messio, S. Bieri, C. Lhuillier, and B. Bernu, Chiral spin liquid on a kagome antiferromagnet induced by the dzyaloshinskii-moriya interaction, Physical Review Letters 118, 267201 (2017).
- [38] K. Mondal and C. Kadolkar, Schwinger boson meanfield theory of the kagome heisenberg antiferromagnet with dzyaloshinskii-moriya interactions, Physical Review B 95, 134404 (2017).
- [39] A. Ralko and J. Merino, Chiral bosonic quantum spin liquid in the integer-spin heisenberg-kitaev model, Physical Review B 110, 134402 (2024).
- [40] D. Sasamoto and J. Nasu, Schwinger boson theory for s = 1 kitaev quantum spin liquids (2025), arXiv:2509.25761 [cond-mat.str-el].
- [41] L.-P. Regnault, C. Boullier, and J. Lorenzo, Polarized-neutron investigation of magnetic ordering and spin dynamics in BaCo2(AsO4)2 frustrated honeycomb-lattice magnet, Heliyon 4, 10.1016/j.heliyon.2018.e00507 (2018), publisher: Elsevier.
- [42] J. C. Halimeh and M. Punk, Spin structure factors of chiral quantum spin liquids on the kagome lattice, Phys. Rev. B 94, 104413 (2016).
- [43] H. Zhang and C. A. Lamas, Exotic disordered phases in the quantum J_1 - J_2 model on the honeycomb lattice, Phys. Rev. B **87**, 024415 (2013).
- [44] D.-V. Bauer and J. O. Fjærestad, Schwinger-boson meanfield study of the J_1-J_2 heisenberg quantum antiferromagnet on the triangular lattice, Phys. Rev. B **96**, 165141 (2017).